Cloud cover and aurora contamination at dome A in 2017 from KLCAM

Xu Yang [ORCID],[1,2] Zhaohui Shang [ORCID],[1,3]★ Keliang Hu,[1] Yi Hu,[1] Bin Ma,[1] Yongjiang Wang,[1,2] Zihuang Cao,[1] Michael C. B. Ashley[4] and Wei Wang[1]

[1]*National Astronomical Observatories, Chinese Academy of Sciences, Beijing 100101, China*
[2]*University of Chinese Academy of Sciences, Beijing 100049, China*
[3]*Tianjin Normal University, Tianjin 300387, China*
[4]*School of Physics, University of New South Wales, Sydney, NSW 2052, Australia*

ABSTRACT

Dome A in Antarctica has many characteristics that make it an excellent site for astronomical observations, from the optical to the terahertz. Quantitative site testing is still needed to confirm the site's properties. In this paper, we present a statistical analysis of cloud cover and aurora contamination from the Kunlun Cloud and Aurora Monitor (KLCAM). KLCAM is an automatic unattended all-sky camera aiming for long-term monitoring of the usable observing time and optical sky background at Dome A. It was installed at Dome A in January 2017, worked through the austral winter, and collected over 47 000 images over 490 d. A semi-quantitative visual data analysis of cloud cover and auroral contamination was carried out by five individuals. The analysis shows that the night sky was free of clouds for 83 per cent of the time, which ranks Dome A highly in a comparison with other observatory sites. Although aurorae were detected somewhere on an image for nearly 45 per cent of the time, the chance of a point on the sky being affected by an aurora is small. The strongest auroral emission lines can be filtered out with customized filters.

Key words: atmospheric effects – instrumentation: miscellaneous – site testing.

1 INTRODUCTION

Dome A is an excellent ground-based astronomical site at the highest point on the Antarctic plateau at an altitude of 4093 m above sea level. It was first visited by the Chinese National Antarctic Research Expedition (CHINARE) in 2005 and is also the place where the Chinese Kunlun Station is located. Various telescopes and astronomical instruments have been installed at Dome A over a 10-yr period for both astronomical observations and site testing (Shang 2020).

Given the harsh environment at Dome A and the fact that Kunlun Station is not currently a winterover station, the development and operation of the telescopes and instruments at Dome A is a great challenge. The equipment must be designed to work unattended and fully automatically for at least a year, with the capability of remote control via very limited bandwidth of Iridium satellite. A good example is the Antarctic Survey Telescopes for time-domain astronomy (AST3; Ma et al. 2020a); the instruments for site testing face the same challenges and requirements.

Many site testing instruments have been installed and operated at Dome A, and the results have shown that Dome A is an exceptional site for astronomical observations. The Surface layer Non-Doppler Acoustic Radar (SNODAR; Bonner et al. 2008) showed that the median thickness of the atmospheric turbulent boundary layer is remarkably thin at 13.9 m̊ (Bonner et al. 2010), allowing the excellent seeing in the free atmosphere to be accessed from a tower of modest height. Ma et al. (2020b) recently confirmed this using the combined

data from the KunLun Differential Motion Monitor (KL-DIMM; Ma et al. 2018) on an 8 m tower and the multilayer Kunlun Automated Weather Station (Hu et al. 2014, 2019) on a 15 m tower. KL-DIMM observed seeing as low as 0.13 arcsec, with a median of 0.31 arcsec (Ma et al. 2020b) when the boundary layer was below the telescope's aperture. In the terahertz (sub-millimetre) regime, instruments such as the prototype High Elevation Antarctic Terahertz telescope (Pre-HEAT; Kulesa et al. 2008), Nigel (Sims et al. 2012a), and the Fourier Transform Spectrometer (FTS; Shi et al. 2016) have shown that the perceptible water vapour at Dome A is extremely low, less than half a millimetre, making the terahertz sky transparency exceptionally good. Other instruments such as Gattini (Moore et al. 2012), Nigel (Sims et al. 2012b), and the Chinese Small Telescope ARray (CSTAR; Zou et al. 2010) have studied the sky background, airglow, and aurora at Dome A. A recent detailed review of astronomy at Dome A, including site testing, can be found in Shang (2020).

Among the key parameters of astronomical site testing, the fraction of clear nights free of clouds is crucial for optical and infrared astronomy. This is particularly important at Dome A where the Antarctic winter provides the opportunity to obtain continuous observations spanning days and weeks. Using 5 months of CSTAR data from Dome A during 2008 winter to define a relative transparency variation, Zou et al. (2010) reported a photometric night (extinction < 0.3 mag) fraction of 67 per cent. The field of view (FOV) of CSTAR was 20 deg^2, centred on the south celestial pole which is about 10° from local zenith. Yang et al. (2017) also estimated the cloud cover at Dome A with Gattini data of 2009. They measured the sky transparency of images and obtained a photometric night fraction of 62.4 per cent, roughly consistent with the CSTAR results, but in a much wide FOV of 90° × 90°, which was also centred on the south

celestial pole. These results show that the photometric night fraction at Dome A is very promising compared to Mauna Kea or northern Chile (Zou et al. 2010). However, the data covered only part of the sky and long-term systematic monitoring was not available.

Several different methods have been developed over the past decades to carry out systematic estimates of clear night fraction. In the early years of site testing, such as for the Very Large Telescope (VLT) Project (Ardeberg 1986), a visual estimate of cloud cover was used. As technology evolved, satellite data reference have also been used to analyse cloud cover in site testing for large projects such as the European Extreme Large Telescope (E-ELT; Kurlandczyk & Sarazin 2017) and the Thirty Meter Telescope (TMT; Schöck et al. 2009). However, the results from satellite data were proven to be reliable only after compared with and verified by ground-based observations (Schöck et al. 2009). Furthermore, satellite images over Antarctica during wintertime have difficulty distinguishing the difference between cloud and the ice surface, since both are a similar temperature and colour. Nowadays, all-sky cameras are usually the best option for ground-based observations of cloud cover, with the obvious advantages that images are recorded frequently and can be analysed systematically. In the case of the site testing for TMT, the All-Sky CAmera (*ASCA*) was used for measuring cloud cover and calibrating the satellite data (Skidmore et al. 2011).

At Dome A, an earlier all-sky camera, the High-Resolution CAMera (HRCAM; Sims et al. 2013) obtained data throughout 2010 (Sims 2013), but coverage in later years was affected by shutter and disc drive failures. To improve the coverage we designed the Kunlun Cloud and Aurora Monitor (KLCAM) to continue the study of both cloud cover and aurora contamination at Dome A.

In Section 2, we present the basic design of KLCAM and the pre-deployment tests we undertook to ensure that KLCAM would work at Dome A. In Section 3, we describe the observation strategy we used with KLCAM, and the data we obtained. The method we use to analyse the data and the results are described in Section 4. In Section 5, we discuss some issues of the work, the advantages and disadvantages of our analysis, and future work.

2 INSTRUMENT

The detailed design of KLCAM can be found in Shang et al. (2018). Here we briefly present the basic features of KLCAM.

KLCAM has a Canon 100D camera equipped with a Sigma 4.5mm f/2.8 fish-eye lens that allows complete coverage of the sky from the zenith to the horizon in all directions. KLCAM is controlled by a customized ARM-based computer. Fig. 1 shows the body of KLCAM with everything inside the metal shell. The thermal design of KLCAM allowed it to work at the low temperatures and low atmospheric pressures at Dome A. The camera sits on an isothermal plate, with a thick insulation layer of low thermal conductivity material between the camera and the low emissivity metal shell. Similarly to the earlier HRCAM, the thermal design forces most of the internal heat to pass through the fish-eye lens, thereby preventing frosting on the lens.

An active heating system keeps the camera temperature between 0 and 10 °C. Because of the good insulation, only 10 watts are needed for heating, even when the ambient temperature drops as low as −80°C. In the case of unexpected problems, we can access the camera remotely via satellite communication.

Before being deployed to Dome A, KLCAM was tested both in the laboratory and in the field. We tested KLCAM down to −70 °C inside a cold chamber and verified that the thermal design could keep the camera temperature above 0 °C. To verify the performance

Figure 1. A photo of KLCAM. On the top is the camera lens. The sockets on the side of the metal shell are for the network connection and power supply.
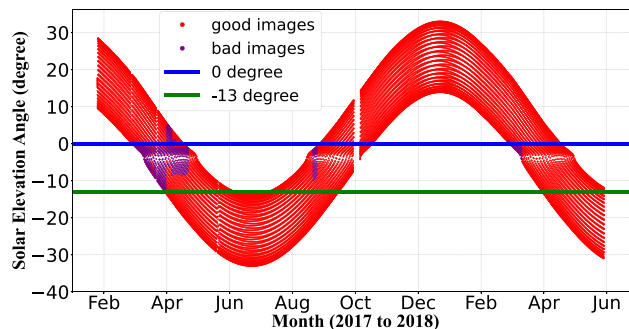

Figure 2. The KLCAM data points shown in the plot of solar elevation angle versus observation date. Each red dot represents one good image, and each purple dot represents one bad image. The blue line indicates the horizon, and the green line marks the solar elevation angle of −13° . There was a 5-d downtime, shown as the small gap in October.

of KLCAM in the low air pressure and unattended environment of Dome A, we tested it at a site with an altitude of 4500 m above sea level. KLCAM worked perfectly during all of these tests and was installed at Dome A in 2017 by the 33rd CHINARE team. The power and Iridium satellite communication for KLCAM as well as other instruments were supported by the automated observatory platform PLATO-A (Ashley et al. 2010).

3 OBSERVATIONS AND DATA

From the date of installation at Dome A in January 2017, KLCAM worked well for 490 d except for a 5-d downtime in October 2017 due to a power issue, shown as the small gap in Fig. 2. KLCAM worked unattended throughout the whole Antarctic winter until PLATO-A ran out of fuel in May 2018.

We developed an observing strategy to balance the frequency of the monitoring and the camera shutter life. The camera of KLCAM is a commercial digital camera with a mechanical shutter which is a

hidden danger for the system in the harsh environment. In addition, KLCAM has to work in a real unattended situation at Dome A, without repairing or replacement for at least 1 yr, and sometimes 2 yr if there is no Dome A expedition by CHINARE for that year. Considering these factors, we decided to take an exposure every 30 min to ensure a 2-yr lifetime. In order to obtain proper exposures, the exposure time was time dependent, which is determined by the elevation angles of the Sun and the Moon, along with the phase of the Moon. We also changed the *ISO*, the sensitivity of the camera sensor, during the daytime or full moon to prevent overexposure. During dawn and dusk, since the sky brightness changes rapidly, we took multiple images with different exposure times as an extra safety to avoid over- or underexposure.

The images were saved in a Solid State Drive (SSD) inside KLCAM itself, and then downloaded to our storage system installed inside PLATO-A as backups (Ma et al. 2020a). From 2017 January 17 to 2018 May 28 before PLATO-A ran out of fuel, a total of 47 035 images were taken covering 485 d (excluding a 5-d gap) as shown in Fig. 2. However, here we are only interested in night-time images, defined as those taken between when twilight started and when twilight ended. At Dome A, twilight occurs when the sun is 13° below the horizon (see Zou et al. 2010). We first excluded 1062 saturated or underexposed bad images, including only two night-time images at the very beginning of the season. When there were multiple exposures at a time, we only kept the best one, excluding 23 953 images in total. After these selections, there are 22 020 images left, of which only 6664 night-time images are used in the following analysis.

4 ANALYSIS AND RESULTS

To analyse the cloud cover and aurora contamination at Dome A, we adopted a method similar to that for TMT site testing to classify the all-sky images by visual analysis.

4.1 TMT method

Site testing for TMT used a visual analysis method of all-sky image, due to the complexity of analysing the images quantitatively. First, they divided each all-sky image into three regions used two circles centred on the local zenith, with the outer one at a zenith angle of 65° and the inner one at 44.7° (Fig. 3). The angles were chosen so that the outer region, which is the annulus between the two circles, has the same sky area as the inner circle, and the third region outside the outer circle is simply ignored because of the observing limit of TMT.

The images were then made into movies, each of which covering an hour of night-time data. Independent analysers then visually inspected and classified the movies into one of the following four pre-defined classes (Skidmore et al. 2011):

(i) `clear` – No clouds are detected inside the 65° zenith angle circle.

(ii) `outer` – Clouds are only detected inside the outer ring (between 65° and 44.7° circles).

(iii) `inner` – Clouds are detected inside the inner 44.7° circle.

(iv) `cover (cloudy)` – Over half of the area inside the 65° circle are covered with clouds.

Finally, the clear (cloud-free) fraction of a site were derived from the statistics on the classification of all data.
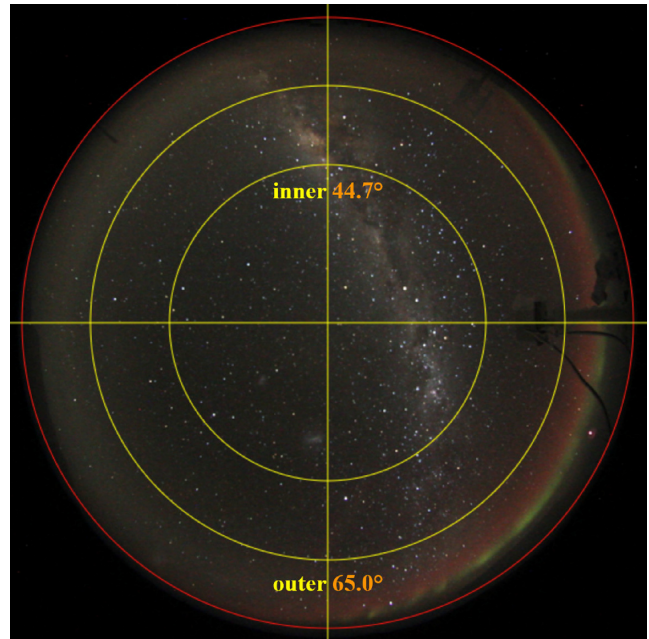

Figure 3. Regions defined on a KLCAM image based on the visual inspection method for TMT site testing. The yellow circles indicate zenith angles of 44.7° and 65°, respectively. The red circle marks the horizon.

4.2 Our modified method

Similar to the TMT method, we have defined four categories of cloud cover for analysing KLCAM images. Instead of using movies, we use individual images, each of which represents half an hour.

As the categories are ordered in a sequence of increasing cloud cover, we assign a number of 1–4 to each category, respectively, and therefore can do the analysis and error estimate semi-quantitatively.

Each image was inspected, classified, and marked independently by five individuals, and the median value was taken as the resultant category of the image. The statistical error can be given by the confusion matrix (Section 4.3). The matrix shows the discrepancy in the classification results from different analysers. For example, if one image is marked as 'clear' by four analysers, and as 'outer' by one analyser, its median value will put it into the result class of 'clear'. In the confusion matrix, there are four counts in the marked class of 'clear' and one count in 'outer', indicating a 20 per cent disagreement with the result class of 'clear'.

Another difference from TMT site testing is that we also need to consider aurora. However, since the cloud and aurora are independent of each other, we can analyse them separately in a similar way, using four categories for aurora contamination.

4.3 Aurora

We analyse aurorae using a similar classification as that of TMT site testing for clouds. Fig. 4 shows examples of the aurora classification described below.

(i) `clear` – No aurorae are detected inside the 65° zenith angle circle.

(ii) `outer` – Aurorae are only detected inside the outer ring (between 65° and 44.7° circle).

(iii) `inner` – Aurorae are detected inside the inner 44.7° circle.

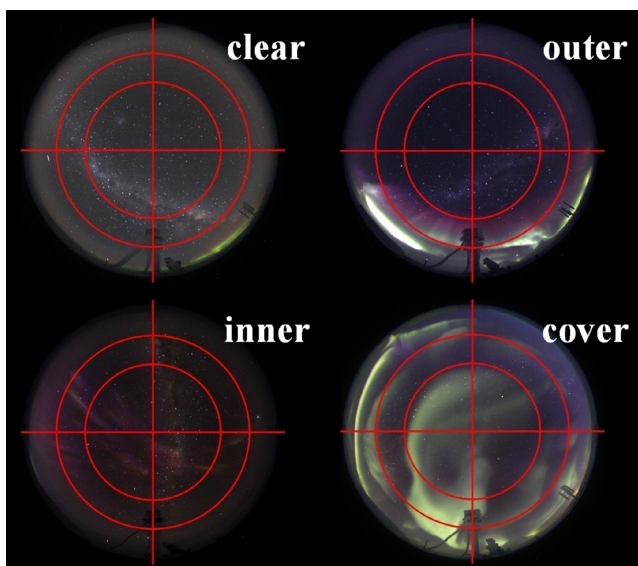(iv) `cover` – Over half of the area inside the 65° circle are covered with aurorae.

Marked Class		Clear	Outer	Inner	Cover		Marked Class		Clear	Light	Heavy	Cover
	Cover	0.0%	0.2%	5.9%	87.6%			Cover	0.0%	0.1%	8.4%	90.4%
	Inner	0.6%	5.2%	86.7%	12.2%			Heavy	0.0%	5.5%	89.8%	9.5%
	Outer	1.5%	86.3%	5.5%	0.2%			Light	1.7%	83.7%	1.5%	0.1%
	Clear	97.9%	8.3%	1.9%	0.0%			Clear	98.3%	10.7%	0.3%	0.0%
Aurora		Clear	Outer	Inner	Cover		Cloud		Clear	Light	Heavy	Cover
		Result Class							Result Class			

Figure 6. Confusion matrices of the statistics for aurora (left) and cloud (right), showing the uncertainties in the result classes due to differences in the classifications from our five human analysers.

86 per cent. For example, in the statistical results for images classified as the 'cover' class, about 12 per cent of them were also marked as the 'inner' class by some analysers. These disagreements result from the fact that some faint aurorae are hard to detect.

As expected, the agreement between the marked classes and a certain result class decreases when the marked one is further from the result one, since each result class actually represents the median of the marked classes as described in Section 4.2. This further demonstrates the robustness of our method.

4.4 Cloud

The situation for cloud analysis is a little different as we cannot use the TMT method since the clouds at Dome A are qualitatively different. Most of the clouds at Dome A are diffuse, so it is hard to classify them as 'inner' or 'outer'. Moreover, one cannot always classify them as 'cover' since there is virtually no real overcast sky and the clouds simply just increase extinction. This was also reported from CSTAR data, where 'cloudy' or worse situation accounted for only 2 per cent of the time, compared to 30 per cent at Mauna Kea (Zou et al. 2010). Therefore, we defined a different classification scheme below, in an attempt to semi-quantitatively characterize the extinction:

(i) clear – No clouds are detected inside the 65° zenith angle circle.

(ii) light – Marginal or minor extinction can be inferred, but the Milky Way is still clear and the stars are bright.

(iii) heavy – High extinctions can be inferred, the number of stars decreases dramatically, or the shape of clouds can be clearly seen.

(iv) cover – Clouds cover all the area and few or no stars can be seen.

Fig. 7 shows examples of our cloud classification and Fig. 5 shows the statistical results. The night sky at Dome A was free of clouds over 83 per cent of the time, and the worst case with 'cover' clouds was only about 3 per cent, consistent with CSTAR results (Zou et al. 2010).

The confusion matrix for cloud statistics in Fig. 5 shows that the classification for 'clear' class is very reliable, with an uncertainty of only 2 per cent among the analysers. The 'heavy' and 'cover' classes have better agreement than corresponding classes in aurora classification, because the effect of heavy extinction on images is easier to be detected by eye than faint aurorae. However, this is not the case for the 'light' class in which different analysers seem to be more inconsistent (about 16 per cent). We attribute this as a subjective effect as the method is semi-quantitative after all.

We compare the night-time clear fraction in different months in 2017 in Fig. 8. Only images that were taken when the sun was 13° below the horizon are shown. As indicated in Fig. 2, we only had 24 h non-stop observations in June and early July. It is good to see that as night-time gets longer, the clear night fraction also increases, to
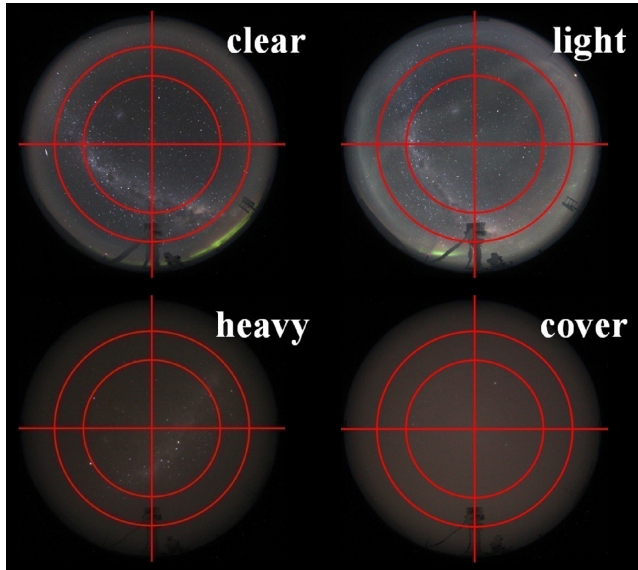
Figure 4. Examples of aurora classification.

Figure 5. Statistical results from visual analysis of cloud and aurora.

We present the statistical results for aurora classification in Fig. 5 together with the results for cloud cover (Section 4.4). Our results show that the sky is free of aurorae for about 55 per cent of the time, as indicated by the 'clear' class. Strong aurorae, marked as 'cover' class, happened for 9 per cent of the time, indicating that such aurorae are not common at Dome A. The remaining 36 per cent of 'inner' and 'outer' classes were usually relatively faint aurorae that are common, as can be seen in Fig. 4. This agrees with the spectroscopic data from NIGEL (Sims et al. 2012b). Since aurorae are composed of only emission lines, customized filters can easily exclude the strong auroral emission lines so as to minimize their contamination to the sky background. Since aurorae only occupy a fraction of the sky, the probability of an observation made with a narrow-field telescope being affected is small. For example, even with an FOV of $4.5° \times 4.5°$, CSTAR images, centered on the south celestial pole, were only affected by aurorae for 2 per cent of the time during the 4-month observing season in 2008 (Zou et al. 2010). However, we did not attempt to estimate this probability in this semi-quantitative work and our future work will study the spatial distribution and probability of the aurorae (Section 5).

Fig. 6 shows the confusion matrix for our uncertainty estimates for aurorae. When there was no aurora, the classifications from our five analysers agree at a level of 98 per cent, indicating a very reliable result. However, when aurorae occurred in the result classes of 'outer', 'inner', and 'cover', the agreements dropped to as low as

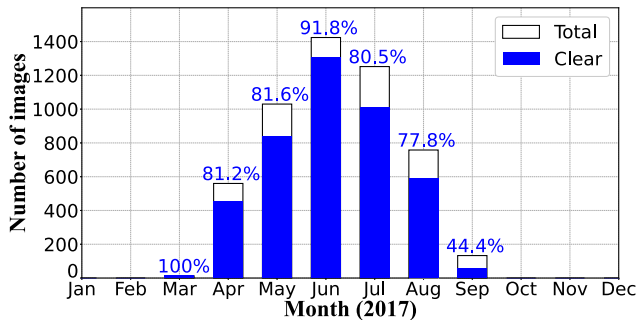**Figure 7.** Examples of cloud classification.

Figure 8. Monthly night-time clear fraction in 2017. The number of total images is proportional to the relative length of the night-time in each month.

more than 90 per cent in June. However, the second half of the winter season does not seem to be as good as the first half, even excluding September when the number of images is small for statistics.

To further investigate the monthly variation, we plot the classification of every image in Fig. 9. It is clear that there were more worse cases in the second half of the season.

However, the above results are based only on data from 2017. Since we have night-time data in May for both 2017 and 2018, we made a simple comparison in Fig. 10. The statistics show similar but different results, with nearly 82 and 86 per cent of 'clear' class for 2017 and 2018, respectively; and about 16 and 12 per cent of 'light' class, respectively. Therefore, we still cannot confirm or rule out any annual variation and need long-term data to do so.

We are confident that our results are not caused by instrument effects, such as frosting on the lens. If frosting was an issue, the frost would build up gradually, but it is clearly not the case for the sudden cloud of 'cover' class in July and August. The design of KLCAM (Section 2) has been proven to be very effective for preventing frosting.

Finally, we compare the night-time clear fraction with those of TMT candidate sites in Table 1. The 83 per cent clear fraction at Dome A seems to be the best among these sites. However, because of the high latitude, although Dome A has the advantage of continuous dark time during polar nights, there is also the disadvantage of fewer

total number of dark hours compared to those sites (Table 1). The annual total number of dark hours at Dome A is only 49 per cent of that at Mauna Kea considering that the general astronomical night starts when the solar elevation angle is $-18°$, and it is 78 per cent when $-13°$ is used for Dome A (Zou et al. 2010).

We also note that the result of this work is semi-quantitative, and we only have 1.5 yr of data.

5 DISCUSSION

As presented in Section 4, although semi-quantitative, our results show good agreement between our five independent analysers. However, visual analysis is still somewhat subjective. In principle, one can even try to tell from a visual inspection of the images whether a night was photometric or spectroscopic, but that would be too subjective and we did not try it. To partially eliminate subjective factors, machine learning and deep learning methods can be employed (Mommert 2020). However, a more complete approach would be to do direct photometry on the all-sky images as mentioned in Sims et al. (2013) and Sims (2013), measuring various parameters for quantitative evaluation of the night sky, such as sky background for aurora contamination, extinction and number of stars for cloud cover.

Once established, these methods will be more efficient and can be applied repeatedly as needed to a future larger data set. For the data set of this work, we expect the new methods to generate more quantitative results, but do not expect our general conclusions to change since the current visual analysis produces relatively robust results as indicated by the confusion matrices.

However, we notice that moonlight could add some uncertainty in our results. It could mostly affect the distinction between the 'clear' and 'light' classes, and has little effect on the 'heavy' or 'cover' classes in which most stars would disappear and there is no confusion. Bright moonlight helps to spot 'light' clouds, and this could possibly result in an underestimate of clouds for moonless nights when 'light' clouds cannot be detected visually. On the other hand, it is also true that when the sky background is high with moonlight, fainter stars are hard to detect in visual inspection and thus a clear sky could be misclassified as 'light' as most analysers are subjectively conservative and strict for 'clear' class. This case is even worse when there were low clouds outside the $65°$ zenith angle circle while the moon was always low, never reaching $30°$ above the horizon during that period. In this scenario, an overestimate of clouds could happen. These complications are also reflected in the confusion matrices where the disagreement in the 'light' classification is the greatest, about 16 per cent. Moreover, in the result class of 'light', there is a 10.7 per cent chance of misclassification towards 'clear', incurring an uncertainty of 1.2 per cent for the 'light' fraction of 11.2 per cent (Fig. 5). Similarly, in the result class of 'clear', there is a 1.7 per cent chance of misclassification towards 'light', giving an uncertainty of 1.4 per cent for the clear fraction of 83.3 per cent. Quantitative analyses mentioned above would eventually get rid of the subjective factors.

Our results show that aurorae could be detected nearly 45 per cent of the time, but they were strong for only 9 per cent of the time. One of the most common and strongest auroral emission lines is the [O I] 557.7 nm line, which is included in the standard *V* band. Sims et al. (2012b) studied the aurorae at Dome A with Nigel and Gattini data, and found that the median auroral contribution to the *V*-band sky brightness is 23.4 mag arcsec^{-2}, while the median value of moonless sky brightness at night is 21.4 mag arcsec^{-2} (Yang et al. 2017). This indicates roughly the extent to which auroral emission lines
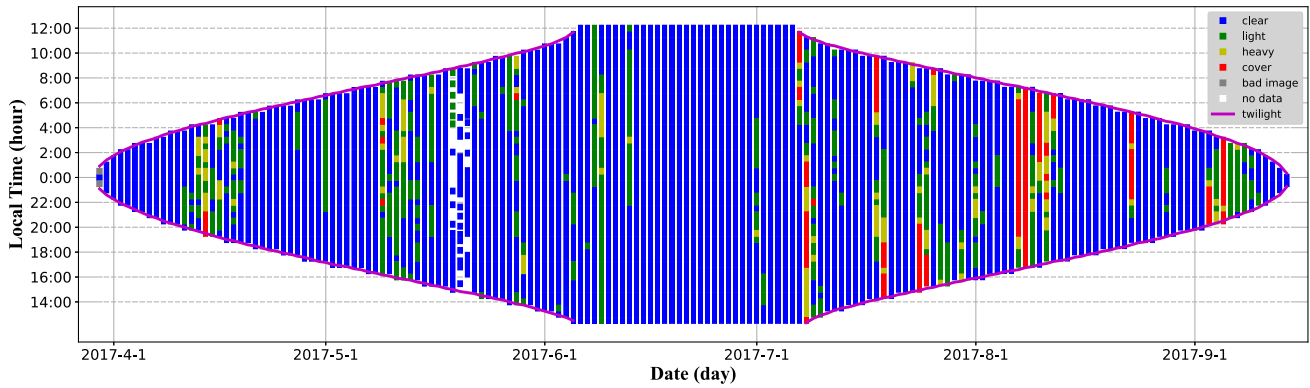
Figure 9. The classification of every night-time image in 2017. Each image is plotted as a small square centred at the local time when it was taken. The irregular missing data during 3 d in May 2017 were due to a software glitch of the Canon camera.
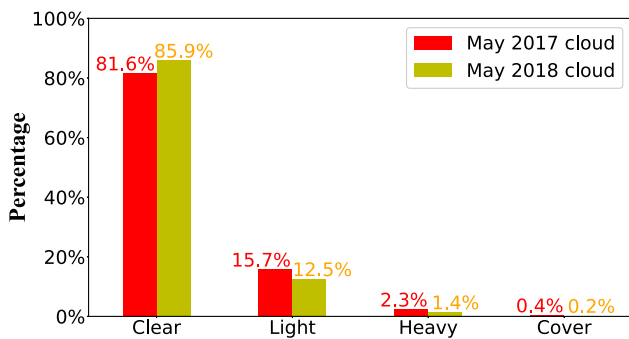

Figure 10. Comparison of the cloud statistics of May in 2017 and 2018.

Table 1. Comparison of clear fraction between Dome A and the TMT candidate sites (Skidmore et al. 2011).

Site	Elevation (m)	Dark Hours[a] (h)	Clear Fraction (per cent)	Clear Dark Hours[b] (h)
Armazones	3064	3392	82	2798
Tolar	2290	3390	77	2624
Tolonchar	4475	3373	72	2442
SPM	2830	3267	73	2372
MK 13N	4050	3390	71	2404
Dome A	4093	2606	83	2136

[a]This refers to the number of annual dark hours defined according to the astronomical twilight when the solar elevation angle is below $-18°$ for TMT sites and $-13°$ for Dome A (Section 3).
[b]The annual clear dark hours are estimated from the clear fraction and the annual dark hours of each site.

contribute to the broad-band sky background. However, as discussed in Section 4.3, the strong auroral emission lines can be excluded by customized filters to minimize the contamination. It has been reported that the aurora contribution to sky brightness at the South Pole can decrease by 1.6 V mag statistically with a notch filter at 557.7 nm, demonstrating the efficiency of specially designed filters (Dempsey, Storey & Phillips 2010).

We also note that aurorae are stronger and appear more in one direction (west to southwest) than the opposite direction. This is because aurorae are mostly from the 'auroral oval' which is a ring shape area centred on the South Geomagnetic Pole as illustrated in Fig. 11. Dome A happens to be located inside the auroral oval and
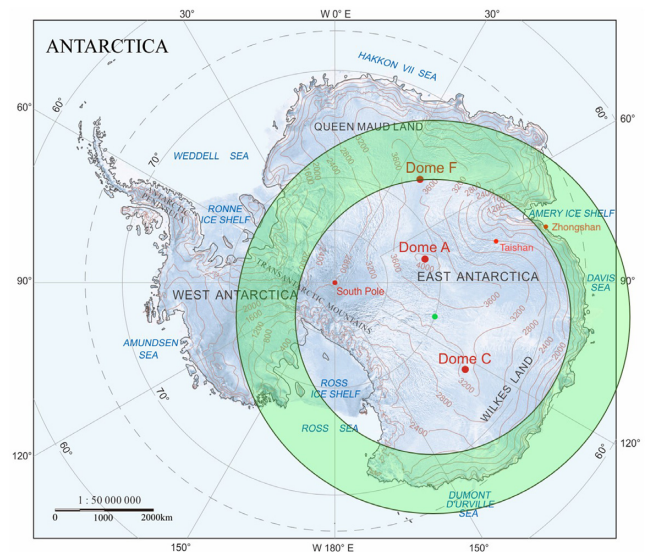

Figure 11. Illustration of the approximate location of the 'auroral oval' centred on the South Geomagnetic Pole (green dot) in Antarctica. Its location varies and does not have a fixed boundary. Original map courtesy of Xiaoping Pang and Shiyun Wang.

so is usually not directly hit by aurorae from the zenith. This is a fortunate situation, and means that visible aurorae generally lie below or close to the horizon at Dome A, leaving less contamination in the sky areas of low airmass than some other Antarctic sites.

Another issue is that when classifying the aurora in Section 4, some images might only have little faint and thin aurorae seen inside the 'inner' area. In such a case, we still mark it as 'inner', the second-worst class, because it would be purely subjective to ignore it by judging its size, or mark it to a different class. Moreover, since we can see the faint aurora, it is possible that the whole area is all contaminated by weaker aurorae, as is a reasonable inference considering the sensitivity of the camera and human eyes. However, in order to keep objective as much as possible, we stuck to what can be seen by human eyes, instead of even reasonable guessing. Future methods discussed above, such as photometry, can also solve this problem.

Finally, KLCAM has an extra function that it can provide real-time observing conditions over the whole sky, and therefore can help to optimize observing plans of the telescopes at Dome A, especially for sky surveys.

6 CONCLUSION

We present the statistical results of the cloud cover and aurora contamination at Dome A using 2017–2018 data from a fully functional all-sky camera KLCAM.

(i) KLCAM was specifically designed and built for the harsh environment at Dome A, Antarctic. It worked well unattended for 490 d since its installation in January 2017 and took 47 035 images.

(ii) In total, 6664 night-time images were visually inspected by five individual analysers and classified into four classes each for cloud cover and aurora contamination.

(iii) We find 83 per cent of time with clear night sky at Dome A, and 55 per cent of time with no aurora at night. Both of these results are reliable with an uncertainty of about 2 per cent based on the confusion matrices.

(iv) The clear fraction at Dome A is slightly better than that at the best candidate site of TMT.

(v) Long-term monitoring is still needed, and more objective analysing methods will be developed to obtain more quantitative systematic results.

DATA AVAILABILITY

The data underlying this article will be shared on reasonable request to the corresponding author.

REFERENCES

Ardeberg A., 1986, in Workshop on ESO's Very Large Telescope, European Southern Observatory Conference and Workshop Proceedings, Vol. 24, ESO, Garching, p. 221
Ashley M. C., Bonner C. S., Everett J. R., Lawrence J. S., Luong-Van D., McDaid S., McLaren C., Storey J. W., 2010, Proc. SPIE, 7735, 773540
Bonner C. S. et al., 2008, Proc. SPIE, 7014, 70146I
Bonner C. S. et al., 2010, PASP, 122, 1122
Dempsey J. T., Storey J. W. V., Phillips A., 2005, PASP, 22, 91
Hu Y. et al., 2014, PASP, 126, 868
Hu Y. et al., 2019, PASP, 131, 015001
Kulesa C. A. et al., 2008, Proc. SPIE, 7012, 701249
Kurlandczyk H., Sarazin M., 2007, Proc. SPIE, 6745, 674507
Ma B., Hu K., Hu Y., Wang W., Shang Z., Wang Y., Yang X., 2018, Proc. SPIE, 10700, 1070052
Ma B. et al., 2020a, MNRAS, 496, 2768
Ma B. et al., 2020b, Nature, 583, 771
Mommert M., 2020, AJ, 159, 178
Moore A. M. et al., 2013, in Burton M. G., Cui X., Tothill N. F. H., eds, Proc. IAU Symp. Vol. 288, Astrophysics from Antarctica. Cambridge Univ. Press, Cambridge, p. 34
Shang Z., 2020, Res. Astron. Astrophys., 20, 168
Shang Z., Hu K., Yang X., Hu Y., Ma B., Wang W., 2018, Proc. SPIE, 10700, 1070057
Schöck M. et al., 2009, PASP, 121, 384
Shi S. C. et al., 2016, Nat. Astron., 1, 0001
Sims G., 2013, PhD thesis, Univ. New South Wales
Sims G. et al., 2012a, PASP, 124, 74
Sims G. et al., 2012b, PASP, 124, 637
Sims G. et al., 2013, in Burton M. G., Cui X., Tothill N. F. H., eds, Proc. IAU Symp. Vol. 288, Astrophysics from Antarctica. Cambridge Univ. Press, Cambridge, p. 38
Skidmore W., Riddle R., Schöck M., Travouillon T., Els S., Walker D., Magnier E., 2011, Rev. Mex. Astron. Astrofis., 41, 70
Yang Y. et al., 2017, AJ, 154, 6
Zou H. et al., 2010, AJ, 140, 602

This paper has been typeset from a TEX/LATEX file prepared by the author.